



ORIGINAL ARTICLE

Quantitative magnetic resonance imaging of the brachial plexus shows specific changes in nerve architecture in chronic inflammatory demyelinating polyneuropathy, multifocal motor neuropathy and motor neuron disease

Marieke H. J. van Rosmalen^{1,2}  | H. Stephan Goedee¹ | Rosina Derks² |
Fay-Lynn Asselman¹ | Camiel Verhamme³ | Alberto de Luca² | J. Hendrikse² |
W. Ludo van der Pol¹ | Martijn Froeling² 

¹Department of Neurology and Neurosurgery, Brain Center Rudolf Magnus, University Medical Center Utrecht, Utrecht, The Netherlands

²Department of Radiology, University Medical Center Utrecht, Utrecht, The Netherlands

³Department of Neurology, Amsterdam Neuroscience, Amsterdam University Medical Centers, University of Amsterdam, Amsterdam, The Netherlands

Correspondence

Martijn Froeling, Department of Radiology, University Medical Center Utrecht Brain Center, Heidelberglaan 100, 3508GA, Utrecht, The Netherlands.
Email: m.froeling@umcutrecht.nl

Funding information

This study was supported by the Prinses Beatrix Spierfonds (W.OR17-21).

Abstract

Background: The immunological pathophysiologicals of chronic inflammatory demyelinating polyneuropathy (CIDP) and multifocal motor neuropathy (MMN) differ considerably, but neither has been elucidated completely. Quantitative magnetic resonance imaging (MRI) techniques such as diffusion tensor imaging, T2 mapping, and fat fraction analysis may indicate in vivo pathophysiological changes in nerve architecture. Our study aimed to systematically study nerve architecture of the brachial plexus in patients with CIDP, MMN, motor neuron disease (MND) and healthy controls using these quantitative MRI techniques.

Methods: We enrolled patients with CIDP ($n = 47$), MMN ($n = 29$), MND ($n = 40$) and healthy controls ($n = 10$). All patients underwent MRI of the brachial plexus and we obtained diffusion parameters, T2 relaxation times and fat fraction using an automated processing pipeline. We compared these parameters between groups using a univariate general linear model.

Results: Fractional anisotropy was lower in patients with CIDP compared to healthy controls ($p < 0.001$), patients with MND ($p = 0.010$) and MMN ($p < 0.001$). Radial diffusivity was higher in patients with CIDP compared to healthy controls ($p = 0.015$) and patients with MND ($p = 0.001$) and MMN ($p < 0.001$). T2 relaxation time was elevated in patients with CIDP compared to patients with MND ($p = 0.023$). Fat fraction was lower in patients with CIDP and MMN compared to patients with MND (both $p < 0.001$).

Conclusion: Our results show that quantitative MRI parameters differ between CIDP, MMN and MND, which may reflect differences in underlying pathophysiological mechanisms.

W. Ludo van der Pol and Martijn Froeling contributed equally to the article.

This is an open access article under the terms of the Creative Commons Attribution-NonCommercial-NoDerivs License, which permits use and distribution in any medium, provided the original work is properly cited, the use is non-commercial and no modifications or adaptations are made.

© 2021 The Authors. *European Journal of Neurology* published by John Wiley & Sons Ltd on behalf of European Academy of Neurology.

KEYWORDS

chronic inflammatory demyelinating polyneuropathy, diffusion tensor imaging, magnetic resonance imaging, multifocal motor neuropathy, pathophysiology

INTRODUCTION

Inflammation of peripheral nerves is the underlying disease mechanism that causes muscle weakness and sensory deficits in chronic inflammatory polyneuropathies, including multifocal motor neuropathy (MMN) and chronic inflammatory demyelinating polyneuropathy (CIDP). MMN is characterized by asymmetric weakness without sensory deficits that dominates in the arms, while CIDP may cause pure motor, pure sensory, or mixed deficits that are most pronounced in the legs. Nerve conduction studies may show conduction blocks and nerve imaging studies have revealed multifocal thickening of nerves in both CIDP and MMN [1,2].

The immunological pathophysiologies of CIDP and MMN differ considerably, but have not been elucidated completely. Autopsy studies, sural nerve biopsy, immunostaining with patient sera *in vitro* and animal models have provided insight into the underlying immunological mechanisms [3-9]. There is an obvious need for additional tools to study the condition of peripheral nerves *in vivo* to further dissect the underlying pathophysiological mechanisms. Quantitative magnetic resonance imaging (MRI) may bridge this gap: diffusion tensor imaging (DTI) and measurements of T2 relaxation times and fat fraction may indicate specific pathophysiological changes in the myelin sheath and axon in patients with CIDP and MMN.

DTI is an MRI technique that provides quantitative parameters as fractional anisotropy (FA), mean diffusivity (MD), axial diffusivity (AD) and radial diffusivity (RD). These parameters give insight into the microstructural integrity of (nervous) tissue and appear to correlate with histological findings [10-13]. Previous DTI studies evaluated peripheral nerves such as the tibial, sciatic and median nerve of patients with CIDP or MMN and healthy controls [14-19]. The brachial plexus was analyzed in a recent exploratory pilot study in a small cohort of patients and showed different FA values between patients with CIDP and MMN [20]. Studies using other quantitative MRI techniques (e.g., T2 mapping or fat fraction analysis) documented an increase in T2 relaxation time in the brachial and lumbosacral plexus and in the tibial nerve in small cohorts of patients with CIDP [21-23]. Complete and systematic studies of the brachial plexus are lacking.

We therefore performed a detailed and systematic quantitative MRI study in a large cohort of patients with CIDP, MMN, motor neuron disease (MND) and healthy controls to compare diffusion parameters, T2 relaxation times and fat fraction of the brachial plexus. The aim of this study was to interpret these results in view of the underlying pathophysiological mechanisms of CIDP and MMN.

METHODS

Study design

We performed a cross-sectional study in patients with CIDP, MMN, MND and healthy controls. We performed quantitative MRI in all patients and used an automated processing pipeline to obtain parameters on microstructural integrity. We compared these parameters between groups and explored correlations with clinical data.

Participants and clinical data

Consecutive patients with CIDP, MMN and MND were included at the outpatient clinic of the University Medical Center Utrecht (UMCU). All prevalent and incident patients with an established diagnosis of CIDP or MMN (definite, probable, possible), according to the predefined consensus criteria of the European Federation of Neurological Societies/Peripheral Nerve Society, were eligible for inclusion [2,24,25]. Patients with MND (i.e., amyotrophic lateral sclerosis [ALS] or progressive muscular atrophy [PMA]), according to the Brooks criteria, were enrolled as disease controls [26]. Healthy controls were included if they had no history of neuromuscular disorders, neuropathy, nerve root injuries or other cervical spine disorders. We excluded patients aged <18 years, patients with atypical forms of CIDP (e.g., Lewis-Sumner syndrome) and patients with MND that had a bulbar onset of symptoms to minimize heterogeneity in these groups, and participants who met one of the routine contraindications for MRI.

We documented demographic and clinical data from all patients, including muscle strength expressed as a Medical Research Council (MRC) sum score. We tested the following 12 muscle groups on both sides: finger flexion, finger extension, finger abduction, wrist flexion, wrist extension, elbow flexion, elbow extension, shoulder abduction, hip flexion, knee flexion, knee extension and foot dorsiflexion. We calculated MRC sum scores of these 24 measurements, ranging from 0 to 120 (normal). The medical ethical committee of the UMCU approved this study (18-349/NL 62866.041.17). This study conforms with the World Medical Association Declaration of Helsinki. Written informed consent was obtained from all study participants.

Equipment and MRI protocol

All participants underwent an MRI scan of the brachial plexus bilaterally in supine position on a 3.0 Tesla MRI scanner (Philips Healthcare, Best, The Netherlands) using a 24-channel head-neck coil. We performed DTI in a transversal slice orientation to obtain diffusion

parameters, T2 mapping in a coronal slice orientation to obtain T2 relaxation times and T1 Dixon in a transverse slice orientation to obtain fat fraction. As an anatomical reference we used a three-dimensional (3D) turbo spin-echo (TSE) spectral presaturation with inversion recovery (SPIR) sequence in a coronal slice orientation. The acquisition parameters are shown in Table 1. We performed a data quality check after the enrollment of 43 participants that showed a higher-than-expected frequency (>5%) of insufficient data due to low signal-to-noise ratios (SNRs). Therefore, we performed DTI twice in all the subsequent participants to improve data quality. These two acquisitions were combined in a later stage during data processing. We excluded scans of low quality, for example, due to movement or the presence of artifacts, from further processing.

Data processing

DTI

We processed all DTI data semi-automatically, using a two-step custom-built processing pipeline based on the diffusion toolbox ExploreDTI which allows visualization of the spinal nerve roots, segmented tract analysis and extraction of diffusion parameters [27]. An overview of the pipeline is shown in Figure 1.

Before processing, we resampled the 3D TSE SPIR to a $2 \times 2 \times 2 \text{ mm}^3$ isotropic resolution. Subsequently, we manually drew a rough mask of the brachial plexus area using ITK SNAP (10 minutes per dataset) [28]. These masks were drawn in the resampled 3D TSE

SPIR and in the diffusion-weighted image to guide the registration and fiber tract selection (Figure 1b). The first automated part of the processing pipeline comprised data denoising, affine registration to correct for subject motion and eddy currents, b-spline registration to correct for echo-planar imaging distortions, tensor estimation using an iterative weighted linear least squares algorithm and whole volume fiber tractography (seed point resolution $1 \times 1 \times 1 \text{ mm}^3$, step size 1 mm, seed FA threshold 0.15, FA track range 0.1–0.8, fiber length range 20–200 mm, angle threshold 15° per step; Figure 1c). This first automated processing step required approximately 35 minutes per dataset to complete.

Next, we manually defined slices with starting and ending points of tracts. Starting points were located next to the ganglion of nerve root C5, C6 and C7, ending points were located five slices further in the distal direction (5 minutes per dataset). This aided a second algorithm to find all tract locations of the nerves using a tract density map (Figure 1d) and specified the appropriate regions of interest (ROIs) for nerve segmentation (Figure 1e). To pair ROIs in the proximal starting and distal ending slices, the algorithm performs a connectivity analysis for all defined ROIs. Every pair of ROIs with high connectivity is then defined as tract bundles which results in a reconstruction of the nerve roots (Figure 1f). Subsequently, the nerve root segments were constructed using the predefined starting and ending slice (Figure 1g). These nerve root segments were used to standardize the site of extraction of diffusion parameters (FA, MD, AD, RD), that is, next to the ganglion over a distance of 1 cm. This second automated part of the pipeline required approximately 5 minutes per dataset to complete.

TABLE 1 Magnetic resonance imaging parameters

Parameter	DTI	T2 mapping	T1 Dixon	3D TSE
Acquisition	2D SE-EPI	2D TSE	3D FFE	3D TSE
Field of view	$240 \times 180 \times 150 \text{ mm}^3$	$240 \times 180 \times 52.5 \text{ mm}^3$	$288 \times 288 \times 200.25 \text{ mm}^3$	$336 \times 336 \times 170 \text{ mm}^3$
Matrix size	96×71	96×96	192×192	224×223
Slice thickness	2.5 mm	2.5 mm	–	–
Voxel size	$2.5 \times 2.5 \times 2.5 \text{ mm}^3$	$2.5 \times 2.5 \times 2.5 \text{ mm}^3$	$0.75 \times 0.75 \times 0.75 \text{ mm}^3$	$0.75 \times 0.75 \times 1 \text{ mm}^3$
Echo time	60 ms	7.6 ms	1.186 ms	206 ms
Number of echoes	–	17	3	–
Repetition time	8595 ms	3242 ms	5615 ms	2200 ms
Flip angle	–	–	16°	–
Turbo spin echo factor	–	–	–	76
Sensitivity encoding factor	2.5	2.3	2 (AP); 1 (FH)	3 (RL); 1.5 (AP)
Fat suppression	SPAIR	–	–	SPIR
Gradient directions	37	–	–	–
b values (s/mm^3)	0, 50, 100, 150, 300, 400, 600	–	–	–
Acquisition time	05:43 min	04:45 min	01:56 min	03:59 min

3D, three dimensional; AP, anterior/posterior; DTI, diffusion tensor imaging; FFE, fast field echo; FH, foot/head; ms, millisecond; RL, right/left; SE-EPI, spin echo-echo planar imaging; SPAIR, spectral attenuated inversion recovery; SPIR, spectral presaturation with inversion recovery; TSE, turbo spin echo.

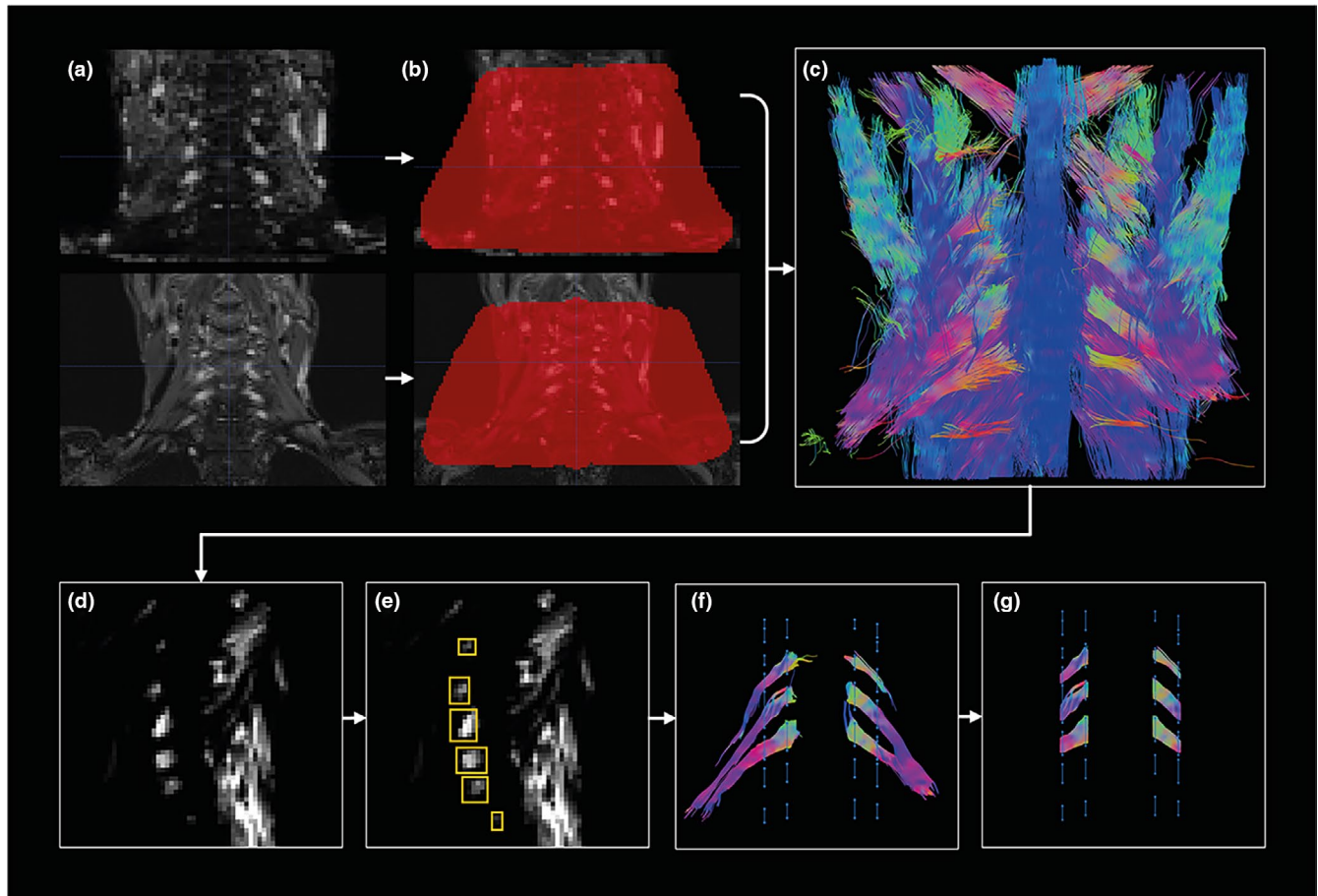


FIGURE 1 Overview of processing pipeline. A diffusion-weighted image and a resampled three-dimensional turbo spin-echo spectral presaturation with inversion recovery sequence are obtained (a, upper and lower image, respectively). After manually drawn masks of the brachial plexus area (b) the automatic processing pipeline results in whole volume fiber tractography (c). Nerve locations are found in a tract density map (d) which specifies region of interests (e). A connectivity analysis results in reconstruction of nerve roots (f) and subsequently in nerve root segments from which diffusion parameters are derived (g) [Colour figure can be viewed at wileyonlinelibrary.com]

Finally, we visually identified and labeled the selected tracts as the left and right nerve roots of C5, C6 or C7 (5 minutes per dataset). If necessary, manual ROIs were placed to optimize the result of the automated data processing (5 minutes per dataset). When no tracts were found, nor with the algorithm, nor manually, the dataset was excluded from further analysis. Finally, diffusion parameters per fiber tract were calculated using tract-based analysis.

T2 mapping and T1 Dixon

Dixon fat fraction maps were calculated using the water and fat image reconstructions of the vendor software. The data obtained with T2 mapping were processed using an extended phase graph fitting approach considering inhomogeneous B_1+ [29,30]. This method accounts for different T2 relaxation times for the water and fat component with the T2 of the fat component fixed to a value calibrated on the subcutaneous fat. Quantitative values of the T2 mapping and T1 Dixon were obtained using the same tract-based analysis used for DTI data. Data underwent registration to the same anatomical

space (3D TSE SPIR image) as the DTI data. We obtained T2 relaxation times in milliseconds (ms) and fat fractions in percentages.

Statistical analysis

For statistical analysis we used SPSS Statistics Version 25 (IBM, Armonk, New York, USA). To compare patient characteristics, we used one-way analysis of variance (ANOVA) for numerical data and a Chi-squared test for categorical data. We compared diffusion parameters, T2 relaxation times and fat fraction per side (i.e., right/left) using a paired sample *t* test and corrected for multiple testing using the Bonferroni method. To analyze diffusion parameters, T2 relaxation times and fat fraction between groups we used an univariate general linear model with the MRI parameters as the dependent variable and the study group as a fixed factor. Tukey's honest significant difference (HSD) test was used to correct for multiple testing. A *p* value <0.05 was considered significant. We analyzed diffusion parameters, T2 relaxation times and fat fraction of all nerve roots together and per nerve root (i.e., C5, C6, C7) separately. Correlations between the quantitative parameters and

clinical data were analyzed using the Pearson correlation coefficient r . We considered $r \leq 0.35$ as a weak correlation, 0.36–0.70 as moderate, 0.70–0.89 as high and ≥ 0.90 as a very high correlation [31].

RESULTS

Participants and clinical data

We enrolled 137 participants based on the inclusion and exclusion criteria. We had to exclude 11 more patients: 2 patients (1.5%) because of claustrophobia during scanning, 2 patients (1.5%) because of a changed diagnosis after inclusion, 1 patient (0.7%) due to movement artifacts that led to low data quality and an additional 6 patients (4.4%; CIDP = 3, MMN = 1, controls = 2) after processing and tract segmentation due to insufficient data quality. We used data from 126 study participants for further analysis (CIDP = 47, MMN = 29, MND = 40 [ALS = 19, PMA = 21], healthy controls = 10). The patient characteristics are summarized in Table 2. Patients with MMN were younger than patients with CIDP and PMA ($p < 0.001$). Other characteristics did not differ significantly between groups.

Semi-automated data processing

After automated processing, we identified 92.9% of all nerve roots (93.3%, 98.4% and 86.9% for C5, C6 and C7, respectively), which increased to 96.0% of C5 nerve roots, 99.6% of C6 nerve roots and 95.6% of C7 nerve roots after additional manual adjustments.

Quantitative MRI parameters

Diffusion parameters, T2 relaxation times and fat fraction did not differ between right and left side of the nerve roots, except for FA in nerve root C7 ($p < 0.001$). This only significant finding did not

influence our data and we therefore decided to combine right and left sides in further analysis.

The same applied to patients with ALS and PMA. There were no significant differences in characteristics between patients with ALS and PMA (p values ranged from 0.075–0.999). We therefore present these data as one group of patients (MND) in further analysis.

Diffusion parameters

The means of all quantitative parameters are summarized in Table 3 and visualized in Figure 2. We found a lower mean FA in patients with CIDP (0.27 [standard deviation (SD) 0.05]) compared to healthy controls (0.30 [SD 0.05]; $p < 0.001$), patients with MND (0.28 [SD 0.04]; $p = 0.010$) and MMN (0.30 [SD 0.06]; $p < 0.001$). FA in patients with MMN and healthy controls was higher compared to patients with MND ($p = 0.002$ and $p = 0.038$, respectively).

We found a higher mean MD in patients with CIDP (1.40×10^{-3} mm²/s [SD 0.20]) compared to patients with MND (1.35×10^{-3} mm²/s [SD 0.20]; $p = 0.008$) and MMN (1.3535×10^{-3} mm²/s [SD 0.23]; $p = 0.027$).

Also, the mean RD was higher in patients with CIDP (1.20×10^{-3} mm²/s [SD 0.19]) compared to healthy controls (1.12 [SD 0.17]; $p = 0.015$), patients with MND (1.14×10^{-3} mm²/s [SD 0.16]; $p = 0.001$) and MMN (1.13×10^{-3} mm²/s [SD 0.20]; $p < 0.001$).

We did not find any significant differences in AD between groups.

T2 relaxation time and fat fraction

We found a longer mean T2 relaxation time in patients with CIDP (42.37 ms [SD 5.36]) compared to patients with MND (41.02 ms [SD 4.81]; $p = 0.023$). The fat fraction was lower in patients with CIDP (40.09% [SD 9.61]; $p < 0.001$) and MMN (39.44% [SD 9.07]; $p < 0.001$) compared to patients with MND (43.62% [SD 9.74]).

TABLE 2 Patient characteristics

Parameter	Inflammatory neuropathy		Motor neuron disease		Healthy controls	p value
	CIDP	MMN	ALS	PMA		
Participants, n	47	29	19	21	10	
Age, years (SD)	64.0 (9.6)	53.7 (11.2)	60.4 (12.3)	65.2 (10.4)	57.4 (7.3)	<0.001*
Male, n (%)	39 (83.0)	27 (93.1)	12 (63.2)	18 (85.7)	7 (70.0)	0.088
Disease duration, months (SD)	34.5 (67.1)	65.1 (82.3)	30.8 (24.3)	57.5 (45.4)	–	0.100
MRC sum score (SD)	111.9 (10.1)	113.8 (4.6)	110.6 (7.9)	107.5 (11.2)	–	0.119

ALS, amyotrophic lateral sclerosis; CIDP, chronic inflammatory demyelinating polyneuropathy; MMN, multifocal motor neuropathy; MRC, Medical Research Council; PMA, progressive muscular atrophy; SD, standard deviation.

*Age differs significantly between patients with MMN and patients with CIDP, and between patients with MMN and patients with PMA. Age, disease duration and MRC sum score are mean.

TABLE 3 Quantitative magnetic resonance imaging parameters per study group and per nerve root

Study group	Nerve root	CIDP	MMN	MND	HC	p 1 CIDP vs. MND	p 2 MMN vs. MND	p 3 CIDP vs. MMN	p 4 HC vs. CIDP	p 5 HC vs. MMN	p 6 HC vs. MND
FA											
All		0.27 (0.05)	0.30 (0.06)	0.28 (0.04)	0.30 (0.05)	0.010*	0.002*	<0.001*	<0.001*	0.999	0.038*
C5		0.26 (0.05)	0.29 (0.05)	0.27 (0.04)	0.29 (0.04)	0.563	0.016*	<0.001*	0.035*	0.997	0.237
C6		0.27 (0.05)	0.29 (0.06)	0.28 (0.04)	0.31 (0.05)	0.135	0.780	0.018*	0.002*	0.383	0.099
C7		0.27 (0.05)	0.30 (0.06)	0.28 (0.05)	0.28 (0.05)	0.234	0.074	<0.001*	0.315	0.655	0.958
MD ($\times 10^{-3}$ mm ² /s)											
All		1.40 (0.20)	1.35 (0.23)	1.35 (0.20)	1.34 (0.17)	0.008*	0.999	0.027*	0.137	0.996	0.998
C5		1.41 (0.21)	1.35 (0.22)	1.35 (0.19)	1.30 (0.21)	0.361	0.999	0.363	0.164	0.802	0.719
C6		1.39 (0.17)	1.35 (0.24)	1.32 (0.16)	1.33 (0.13)	0.060	0.837	0.481	0.589	0.993	0.991
C7		1.41 (0.23)	1.35 (0.22)	1.36 (0.23)	1.39 (0.16)	0.477	0.977	0.294	0.963	0.898	0.972
AD ($\times 10^{-3}$ mm ² /s)											
All		1.81 (0.24)	1.79 (0.30)	1.77 (0.28)	1.78 (0.20)	0.224	0.817	0.833	0.849	0.996	0.982
C5		1.81 (0.27)	1.79 (0.30)	1.77 (0.31)	1.72 (0.24)	0.766	0.976	0.971	0.574	0.799	0.906
C6		1.80 (0.19)	1.78 (0.31)	1.74 (0.21)	1.80 (0.15)	0.256	0.711	0.938	1.000	0.991	0.727
C7		1.82 (0.27)	1.79 (0.29)	1.80 (0.32)	1.82 (0.19)	0.922	0.999	0.966	1.000	0.989	0.978
RD ($\times 10^{-3}$ mm ² /s)											
All		1.20 (0.19)	1.13 (0.20)	1.14 (0.16)	1.12 (0.17)	0.001*	0.970	<0.001*	0.015*	0.996	0.949
C5		1.20 (0.19)	1.13 (0.20)	1.14 (0.15)	1.08 (0.19)	0.174	0.933	0.069	0.054	0.841	0.578
C6		1.19 (0.17)	1.13 (0.22)	1.11 (0.15)	1.10 (0.14)	0.026*	0.918	0.225	0.205	0.922	0.997
C7		1.21 (0.21)	1.12 (0.20)	1.15 (0.19)	1.17 (0.16)	0.216	0.871	0.049*	0.853	0.786	0.973
T2 relaxation time (ms)											
All		42.37 (5.36)	41.12 (5.18)	41.02 (4.81)	41.32 (6.72)	0.023*	0.998	0.072	0.626	0.996	0.986
C5		41.97 (5.29)	40.54 (5.43)	40.47 (4.59)	41.00 (8.81)	0.279	1.000	0.413	0.923	0.992	0.986
C6		42.85 (4.65)	41.86 (5.35)	41.78 (4.63)	42.06 (5.10)	0.482	1.000	0.613	0.943	0.999	0.997
C7		42.27 (6.14)	40.90 (4.75)	40.75 (5.16)	40.90 (6.15)	0.319	0.999	0.471	0.826	1.000	1.000
Fat fraction (%)											
All		40.09 (9.61)	39.44 (9.07)	43.62 (9.74)	40.55 (10.33)	<0.001*	<0.001*	0.904	0.991	0.908	0.266
C5		38.51 (8.39)	37.23 (8.29)	42.56 (8.46)	38.16 (10.68)	0.014*	0.004*	0.823	0.999	0.984	0.292
C6		38.54 (8.97)	37.55 (8.75)	42.09 (9.02)	39.62 (9.52)	0.051	0.020*	0.911	0.975	0.865	0.777
C7		43.53 (10.71)	43.37 (8.90)	46.35 (11.16)	43.87 (10.62)	0.335	0.368	1.000	0.999	0.998	0.848

Mean diffusion parameters, T2 relaxation time and fat fraction with standard deviation per study group and per nerve root with calculated p values. p value 1 = CIDP vs. MND; p value 2 = MMN vs. MND; p value 3 = CIDP vs. MMN; p value 4 = HC vs. CIDP; p value 5 = HC vs. MMN; p value 6 = HC vs. MND. Significant differences are indicated with an asterisk (*).

AD, axial diffusivity; CIDP, chronic inflammatory demyelinating polyneuropathy; FA, fractional anisotropy; HC, healthy control; MD, mean diffusivity; MMN, multifocal motor neuropathy; MND, motor neuron disease; ms, millisecond; RD, radial diffusivity.

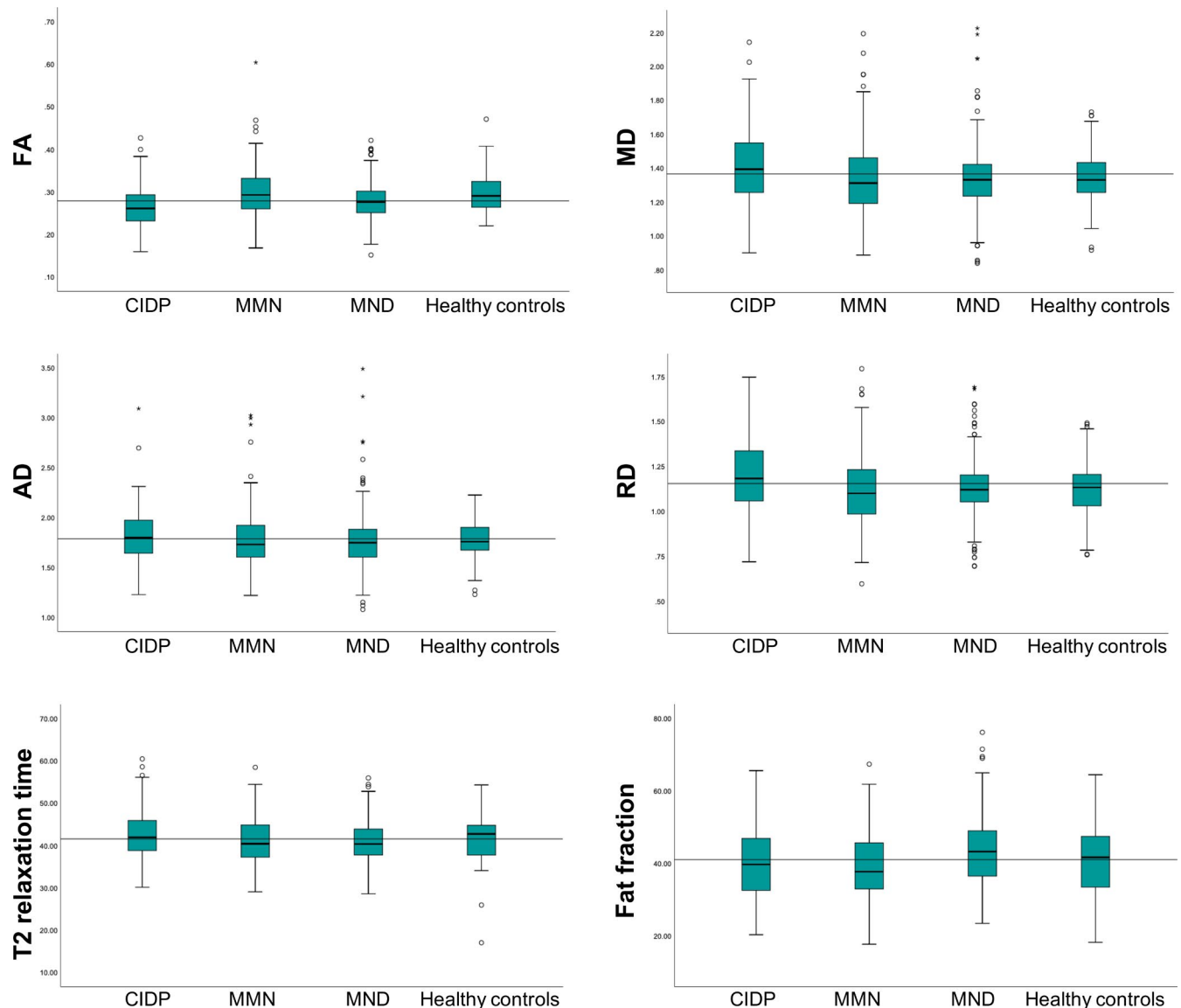


FIGURE 2 Boxplots of quantitative parameter per study group. Boxplots of diffusion parameters, T2 relaxation times and fat fraction with grand mean are shown. MD, AD and RD values are $\times 10^{-3}$ mm²/second, T2 relaxation time is in milliseconds and fat fraction is a percentage. AD, axial diffusivity; CIDP, chronic inflammatory demyelinating polyneuropathy; FA, fractional anisotropy; MD, mean diffusivity; MMN, multifocal motor neuropathy; MND, motor neuron disease; RD, radial diffusivity [Colour figure can be viewed at wileyonlinelibrary.com]

Correlation with clinical data

For all four study groups (CIDP, MMN, MND and healthy controls) we only found weak correlations between the MRI metrics (i.e., diffusion parameters, T2 relaxation time and fat fraction) and the clinical covariates (i.e., age, MRC sum score and disease duration) (Figure 3).

For the correlation with age, r ranged from -0.19 to 0.14 for patients with CIDP, -0.35 to 0.31 for patients with MMN, -0.20 to 0.34 for patients with MND and -0.18 to 0.24 for healthy controls. For MRC sum score, r ranged from -0.23 to 0.10 for patients with CIDP, -0.08 to 0.24 for patients with MMN and -0.13 to 0.20 for patients with MND. For disease duration, r ranged from -0.24 to

0.25 for patients with CIDP, -0.21 to 0.23 for patients with MMN and 0.02 to 0.23 for patients with MND.

DISCUSSION

In this study we show that quantitative MRI techniques reveal differences in the brachial plexus between patients with CIDP, MMN, MND and healthy controls. CIDP is characterized by lower FA and higher RD than MMN, MND and healthy controls, whilst MMN is characterized by higher FA values than CIDP and MND. Patients with MMN and healthy controls did not differ. These differences between CIDP and MMN are the most remarkable and important

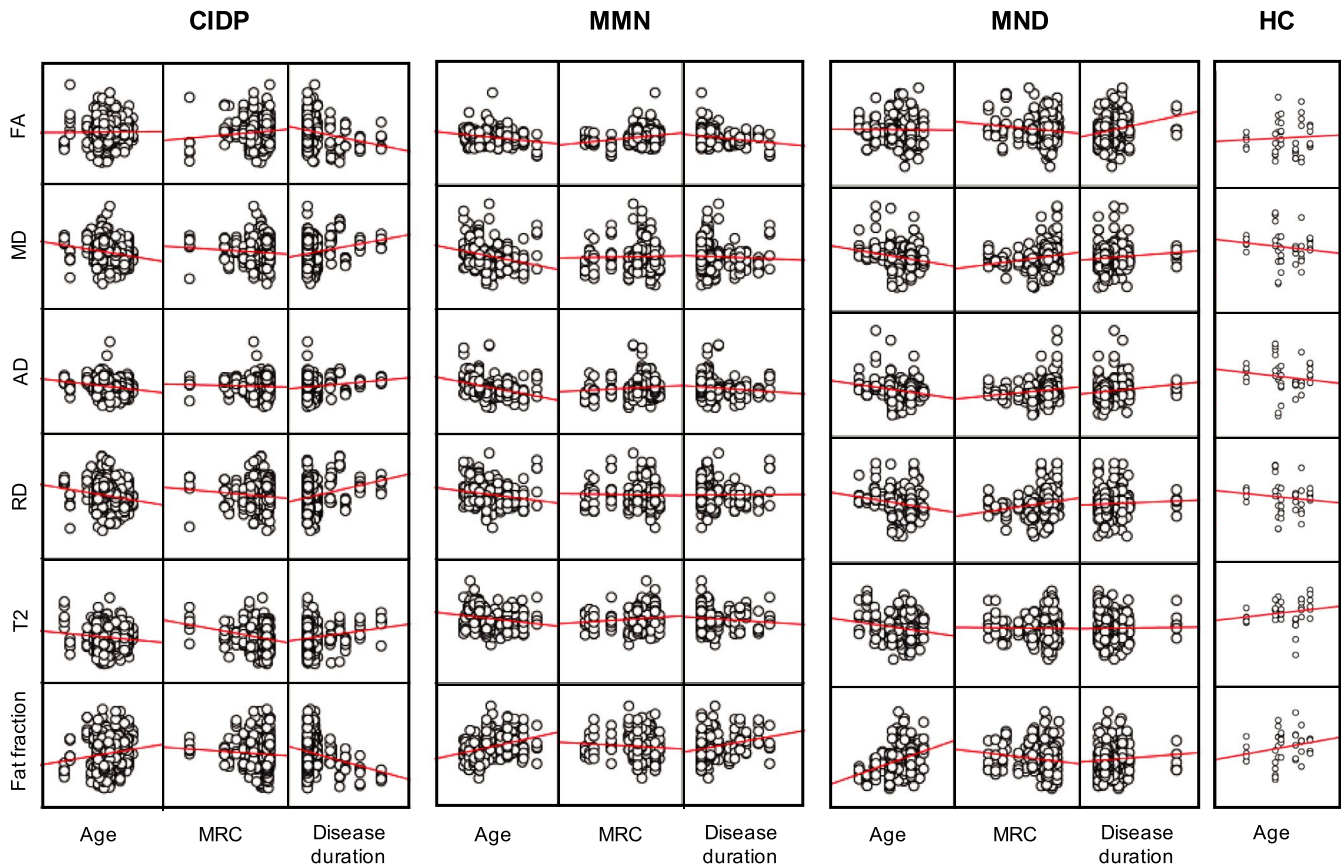


FIGURE 3 Correlation matrix of quantitative parameters with clinical data per study group. Correlation matrix of the MRI metrics FA, MD, AD, RD, T2 and fat fraction (y-axis) with the clinical covariates age, MRC sum score and disease duration (x-axis), shown per study group. AD, axial diffusivity; CIDP, chronic inflammatory demyelinating polyneuropathy; FA, fractional anisotropy; HC, healthy controls; MD, mean diffusivity; MMN, multifocal motor neuropathy; MND, motor neuron disease; MRC, Medical Research Council; RD, radial diffusivity [Colour figure can be viewed at wileyonlinelibrary.com]

finding as they emphasize important differences in the underlying pathophysiology.

This is the first comparative quantitative MRI study in a relatively large cohort of patients with CIDP and MMN. Diffusion parameters obtained from the sciatic, tibial, median, ulnar and radial nerves were previously reported in smaller cohorts [14-17,19]. The absolute differences in the measured parameters are around 2% between study groups, which indicates that differences are probably only found in larger groups. However, the finding of a decreased FA and an increased RD in our study patients with CIDP is in agreement with previous findings, indicating that this DTI profile is characteristic for CIDP and can be found throughout the peripheral nervous system [14-17,19]. Experimental animal studies showed that increased RD may correspond with loss of myelin integrity [10-12]. The combination of decreased FA and increased RD has also been reported in patients with Guillain-Barré syndrome and demyelinating types of Charcot-Marie-Tooth disease, which corroborates that this reflects the disturbance of myelin integrity in peripheral nerves caused by inflammation [32-35]. The longer T2 relaxation times and lower fat fraction in the CIDP cohort compared to the MND cohort indicate the presence of free water, which may also be due to inflammation, and have also been reported at the lumbosacral plexus [21,22,36].

Although decreased FA in combination with increased RD is a robust finding in patients with CIDP, absolute diffusion values differ between proximal and distal nerve sites [14-17,19]. This is probably explained by the proximal to distal decrease in the diameter of fascicles with a corresponding increase in the density of the periaxonal connective tissue [37]. In the well-organized tissues of the distal peripheral nerves, water molecule movement is more restricted in specific directions, which results in larger isotropic diffusion and a higher FA. The FA values of the brachial plexus in our study were lower than in previous studies of distal peripheral nerves in arms and legs, which is in line with this hypothesis [14-17,19].

FA and MD are summary measures from eigenvalues. Changes in FA and MD are therefore driven by changes in AD or RD. In CIDP, the increase in RD seems to drive the changes in FA and MD. RD indicates less hindrance of diffusion for water perpendicular to the nervous tissue. This can be the result of various cellular mechanisms, such as demyelination or a disturbance of the cytoskeleton caused by a loss of neurofilaments and microtubules. We think that our findings may reflect demyelination rather than a disturbance of the cytoskeleton as histological studies reported myelin detachment and myelin loss without damage to axons induced by macrophages around the (inter)nodal regions in patients with CIDP [3-5,38-41].

The mechanism of paranodal myelin detachment is present in some patients with CIDP, as described in earlier electrophysiological studies [42-44]. Taken together, the changes in FA, MD and RD in our CIDP group most likely reflect the loss of myelin.

The absence of increased RD values in patients with MMN indicates that the underlying pathophysiological mechanism is different to that in CIDP and that demyelination is probably not the dominant pathophysiological process. Patients with MMN seem to have comparable quantitative MRI parameters to healthy controls. Scarce histological reports describe normal myelin sheets [6-8]. Electrophysiological studies may support the idea of changed axon structure with largely intact myelin sheets [44]. However, it is rather remarkable that such different DTI profiles are found between patients with MMN and CIDP while diagnostic tools used in clinical practice, such as nerve conduction studies, nerve ultrasound and qualitative MRI of the brachial plexus, may show similar abnormalities, for example, conduction blocks and thickening of the nerves. The differences in DTI profiles indicate that these abnormalities are more likely to present common endpoints of different pathophysiological mechanisms rather than comparable etiologies.

In a previous study we found lower AD in the median and ulnar nerves in the forearm of patients with MMN compared to healthy controls and patients with ALS [18]. It is assumed that AD correlates with axonal loss, for example, due to axonal swelling due to the breakdown or change in the permeability of the axolemma, which is an important feature of MMN [11,45,46]. We did not detect differences in AD between groups at the brachial plexus in this study, which can be explained by the fact that longer axons and distal parts of axons are more susceptible to injury than short and proximal parts of axons. Consequently, AD may remain relatively unchanged in the proximal spinal nerve roots of the brachial plexus. In the previous study we did not find a significant difference in FA between patients with MMN and ALS, although absolute values of FA were higher in patients with MMN [18]. We found a significantly higher FA in patients with MMN compared to patients with MND in this study, which can be explained by the larger sample size and higher statistical power in the current study.

Correlations between clinical data and quantitative MRI parameters were weak. We refrained from studying correlations of nerve conduction studies and imaging results since the measurement sites did not match. More general, imaging and electrophysiological studies may reveal different pathophysiological dimensions. Previous studies found that imaging results did not correlate with nerve conduction study results in cohorts of patients with inflammatory neuropathies [47-51].

A limitation of our study is the effect of partial volume, which may lead to an underestimation of diffusion parameters and fat fraction, and varying SNR which may lead to higher FA and lower RD in case of lower SNRs [52]. However, the influence of partial volume effects and different SNR values were probably small as our results in DTI analysis, T2 mapping and fat fraction analysis are consistent with each other, and scans were performed in random order with the same software versions. Another limitation might be the

registration step in the processing pipeline. Due to an imperfect registration some tracts were not or incompletely found, particularly in nerve root C7 due to strong susceptibility artifacts caused by the lungs. Our healthy control group is small but we think the number of healthy controls is sufficient as standard deviations of the means of the quantitative MRI parameters were small and comparable to the other three study groups, indicating low levels of variation between individuals. Moreover, the diffusion parameters that we observed were similar to those previously reported in the literature [53]. We analyzed relatively short segments of the brachial plexus, since analysis of longer tracts resulted in a significant dropout of data due to poor data quality. We therefore decided to only analyze the first centimeter next to the ganglion in order to maximize the number of datasets. Although we could not include the more distal parts of the brachial plexus, the advantage of this approach is a well-powered study that provides information on a large patient population derived with an automated pipeline without subjective bias.

In conclusion, our study gives insight into the nerve architecture of the brachial plexus in a relatively large cohort of patients with CIDP, MMN, MND and healthy controls. Our study shows that diffusion parameters differ between CIDP and MMN, which may reflect differences in the underlying pathophysiological mechanisms. Future studies should combine assessments of the brachial plexus and distal nerves and assess correlations between quantitative MRI parameters in roots, fascicles and peripheral nerves and specific clinical deficits. They should also address whether changes occur in the disease course or after treatment.

CONFLICT OF INTEREST

M.H.J.v.R., R.A.D., F.-L.A., A.d.L. and M.F. report no competing interests. H.S.G. has received research support from the Prinses Beatrix Spierfonds. J.H. has received research support from the Netherlands Organization for Scientific Research (NWO) under grant no. 91712322 and the European Research Council under grant agreements no. 637024. C.V. is a member of a clinical advisory board (CAB) of Inflectis France; payment was made to his organization for attending a CAB meeting, outside of the submitted work. W.L.v.d.P. has received support from the Prinses Beatrix Spierfonds and Stichting Spieren voor Spieren.

AUTHOR CONTRIBUTIONS

Marieke H. J. van Rosmalen: Conceptualization (equal); Data curation (lead); Formal analysis (lead); Investigation (lead); Methodology (lead); Project administration (supporting); Writing-original draft (lead); Writing-review & editing (equal). **H. Stephan Goedee:** Conceptualization (lead); Data curation (supporting); Formal analysis (supporting); Funding acquisition (lead); Methodology (supporting); Supervision (supporting); Writing-review & editing (supporting). **Rosina A. Derks:** Data curation (equal); Investigation (equal); Methodology (equal); Software (equal); Writing-review & editing (supporting). **Fay-Lynn Asselman:** Project administration (lead); Resources (equal); Writing-review & editing (supporting). **Camiel Verhamme:** Conceptualization (supporting); Investigation

(supporting); Methodology (supporting); Writing-review & editing (supporting). **Alberto de Luca:** Data curation (supporting); Investigation (supporting); Methodology (supporting); Software (lead); Writing-review & editing (supporting). **J. Hendrikse:** Conceptualization (lead); Formal analysis (supporting); Funding acquisition (lead); Methodology (supporting); Writing-review & editing (supporting). **W. Ludo van der Pol:** Conceptualization (lead); Funding acquisition (lead); Methodology (lead); Supervision (lead); Writing-review & editing (lead). **Martijn Froeling:** Conceptualization (lead); Data curation (supporting); Formal analysis (supporting); Investigation (supporting); Methodology (lead); Software (lead); Writing-review & editing (lead).

DATA AVAILABILITY STATEMENT

The data that support the findings of this study are available on request from the corresponding author.

ORCID

Marieke H. J. van Rosmalen  <https://orcid.org/0000-0003-3959-1373>

Martijn Froeling  <https://orcid.org/0000-0003-3841-0497>

REFERENCES

- Allen JA, Lewis RA. CIDP diagnostic pitfalls and perception of treatment benefit. *Neurology*. 2015;85:498-504. <https://doi.org/10.1212/WNL.0000000000001833>
- Vlam L, Van Der Pol WL, Cats EA, et al. Multifocal motor neuropathy: diagnosis, pathogenesis and treatment strategies. *Nat Rev Neurol*. 2012;8:48-58.
- Matthews WB, Howell DA, Hughes RC. Relapsing corticosteroid-dependent polyneuritis. *J Neurol Neurosurg Psychiatry*. 1970;33:330-337.
- Torvik A, Lundar T. A case of chronic demyelinating polyneuropathy resembling the Guillan-Barré Syndrome. *J Neurol Sci*. 1977;32:45-52.
- Matsuda M, Ikeda SI, Sakurai S, Nezu A, Yanagisawa N, Inuzuka T. Hypertrophic neuritis due to chronic inflammatory demyelinating polyradiculoneuropathy (CIDP): a postmortem pathological study. *Muscle Nerve*. 1996;19:163-169. [https://doi.org/10.1002/\(SICI\)1097-4598\(199602\)19:2<163:AID-MUS6>3.0.CO;2-C](https://doi.org/10.1002/(SICI)1097-4598(199602)19:2<163:AID-MUS6>3.0.CO;2-C)
- Krarpur C, Stewart JD, Sumne AJ, Pestronk A, Lipton SA. A syndrome of asymmetric limb weakness with motor conduction block. *Neurology*. 1990;40:118-127. <https://doi.org/10.1212/wnl.40.1.118>
- Adams D, Kuntzer T, Steck AJ, Lohrman A, Janzer RC, Regli F. Motor conduction block and high titres of anti-GM1 ganglioside antibodies: pathological evidence of a motor neuropathy in a patient with lower motor neuron syndrome. *J Neurol Neurosurg Psychiatry*. 1993;56:982-987. <https://doi.org/10.1136/jnnp.56.9.982>
- Veugelers B, Theys P, Lammens M, Van Hees J, Robberecht W. Pathological findings in a patient with amyotrophic lateral sclerosis and multifocal motor neuropathy with conduction block. *J Neurol Sci*. 1996;136:64-70. [https://doi.org/10.1016/0022-510X\(95\)00295-D](https://doi.org/10.1016/0022-510X(95)00295-D)
- Harschnitz O, van den Berg LH, Johansen LE, et al. Autoantibody pathogenicity in a multifocal motor neuropathy induced pluripotent stem cell-derived model. *Ann Neurol*. 2016;80:71-88. <https://doi.org/10.1002/ana.24680>
- Song SK, Sun SW, Ramsbottom MJ, Chang C, Russell J, Cross AH. Demyelination revealed through MRI as increased radial (but unchanged axial) diffusion of water. *NeuroImage*. 2002;17:1429-1436. <https://doi.org/10.1006/nimg.2002.1267>
- Song SK, Sun SW, Ju WK, Lin SJ, Cross AH, Neufeld AH. Diffusion tensor imaging detects and differentiates axon and myelin degeneration in mouse optic nerve after retinal ischemia. *NeuroImage*. 2003;20:1714-1722. <https://doi.org/10.1016/j.neuroimage.2003.07.005>
- Morisaki S, Kawai Y, Umeda M, et al. In vivo assessment of peripheral nerve regeneration by diffusion tensor imaging. *J Magn Reson Imaging*. 2011;33:535-542. <https://doi.org/10.1002/jmri.22442>
- Jeon T, Fung MM, Koch KM, Tan ET, Sneag DB. Peripheral nerve diffusion tensor imaging: overview, pitfalls, and future directions. *J Magn Reson Imaging*. 2018;47:1171-1189. <https://doi.org/10.1002/jmri.25876>
- Kakuda T, Fukuda H, Tanitame K, et al. Diffusion tensor imaging of peripheral nerve in patients with chronic inflammatory demyelinating polyradiculoneuropathy: a feasibility study. *Neuroradiology*. 2011;53:955-960. <https://doi.org/10.1007/s00234-010-0833-z>
- Mathys C, Aissa J, Zu Hörste GM, et al. Peripheral neuropathy: assessment of proximal nerve integrity by diffusion tensor imaging. *Muscle Nerve*. 2013;48:889-896.
- Markvardsen LH, Vaeggemose M, Ringgaard S, Andersen H. Diffusion tensor imaging can be used to detect lesions in peripheral nerves in patients with chronic inflammatory demyelinating polyneuropathy treated with subcutaneous immunoglobulin. *Neuroradiology*. 2016;58:745-752. <https://doi.org/10.1007/s00234-016-1692-z>
- Kronlage M, Pitarokouli K, Schwarz D, et al. Diffusion tensor imaging in chronic inflammatory demyelinating polyneuropathy: diagnostic accuracy and correlation with electrophysiology. *Invest Radiol*. 2017;52:701-707. <https://doi.org/10.1097/RLI.0000000000000394>
- Haakma W, Jongbloed BA, Froeling M, et al. MRI shows thickening and altered diffusion in the median and ulnar nerves in multifocal motor neuropathy. *Eur Radiol*. 2017;27:2216-2224. <https://doi.org/10.1007/s00330-016-4575-0>
- Lichtenstein T, Sprenger A, Weiss K, et al. MRI biomarkers of proximal nerve injury in CIDP. *Ann Clin Transl Neurol*. 2018;5:19-28. <https://doi.org/10.1002/acn3.502>
- Oudeman J, Eftimov F, Strijkers GJ, et al. Diagnostic accuracy of MRI and ultrasound in chronic immune-mediated neuropathies. *Neurology*. 2020;94:e62-e74.
- Hiwatashi A, Togao O, Yamashita K, et al. Lumbar plexus in patients with chronic inflammatory demyelinating polyradiculoneuropathy: evaluation with simultaneous T2 mapping and neurography method with SHINKEI. *Br J Radiol*. 2018;91:20180501.
- Hiwatashi A, Togao O, Yamashita K, et al. Simultaneous MR neurography and apparent T2 mapping in brachial plexus: evaluation of patients with chronic inflammatory demyelinating polyradiculoneuropathy. *Magn Reson Imaging*. 2018;55:112-117.
- Felisz PF, Poli A, Vitale R, et al. MR microneurography and quantitative T2 and DP measurements of the distal tibial nerve in CIDP. *J Neurol Sci*. 2019;400:15-20.
- Van den Bergh PYK, Hadden RDM, Bouche P, et al. European Federation of Neurological Societies/Peripheral Nerve Society Guideline on management of chronic inflammatory demyelinating polyradiculoneuropathy: report of a joint task force of the European Federation of Neurological Societies and the Peripheral Nerve Society – first revision. *Eur J Neurol*. 2010;17:356-363.
- Van Schaik IN, Léger JM, Nobile-Orazio E, et al. European Federation of Neurological Societies/Peripheral Nerve Society guideline on management of multifocal motor neuropathy. Report of a joint task force of the European Federation of Neurological Societies and the Peripheral Nerve Society – first revision. *J Peripher Nerv Syst*. 2010;15:295-301.

26. Brooks BR, Miller RG, Swash M, Munsat TL. El Escorial revisited: revised criteria for the diagnosis of amyotrophic lateral sclerosis. *ALS Mot Neuron Disord*. 2000;1:293-299. <https://doi.org/10.1080/146608200300079536>
27. Leemans A, Jeurissen B, Sijbers J, Jones DK. ExploreDTI: a graphical toolbox for processing, analyzing, and visualizing diffusion MR data. *Proc Int Soc Magn Reson Med*. 2009;17:3537.
28. Yushkevich PA, Piven J, Hazlett HC, et al. User-guided 3D active contour segmentation of anatomical structures: significantly improved efficiency and reliability. *NeuroImage*. 2006;31:1116-1128. <https://doi.org/10.1016/j.neuroimage.2006.01.015>
29. Marty B, Baudin PY, Reyngoudt H, et al. Simultaneous muscle water T2 and fat fraction mapping using transverse relaxometry with stimulated echo compensation. *NMR Biomed*. 2016;29:431-443. <https://doi.org/10.1002/nbm.3459>
30. Keene KR, Beenakker JWM, Hooijmans MT, et al. T2 relaxation-time mapping in healthy and diseased skeletal muscle using extended phase graph algorithms. *Magn Reson Med*. 2019;2020:1-15. <https://doi.org/10.1002/mrm.28290>
31. Taylor R. Interpretation of the correlation coefficient: a basic review. *J Diagnostic Med Sonogr*. 1990;1:35-39.
32. Cao J, He B, Wang S, et al. Diffusion tensor imaging of tibial and common peroneal nerves in patients with Guillain-Barre syndrome: a feasibility study. *J Magn Reson Imaging*. 2019;49(5):1356-1364. <https://doi.org/10.1002/jmri.26324>
33. Vaeggemose M, Vaeth S, Pham M, et al. Magnetic resonance neurography and diffusion tensor imaging of the peripheral nerves in patients with Charcot-Marie-Tooth Type 1A. *Muscle Nerve*. 2017;56:78-84. <https://doi.org/10.1002/mus.25691>
34. Kim HS, Yoon YC, Choi B-O, Jin W, Cha JG, Kim J-H. Diffusion tensor imaging of the sciatic nerve in Charcot-Marie-Tooth disease type I patients: a prospective case-control study. *Eur Radiol*. 2019;1-12: <https://doi.org/10.1007/s00330-018-5958-1>
35. Chhabra A, Carrino JA, Farahani SJ, et al. Whole-body MR neurography: prospective feasibility study in polyneuropathy and Charcot-Marie-Tooth disease. *J Magn Reson Imaging*. 2016;44(6):1513-1521. <https://doi.org/10.1002/jmri.25293>
36. McRobbie DW, Moore EA, Graves MJ. MRI from picture to proton. *Am J Roentgenol*. 2004;182(3):592. <https://doi.org/10.2214/ajr.182.3.1820592>
37. Bonnel F. Microscopic anatomy of the adult human brachial plexus: an anatomical and histological basis for microsurgery. *Microsurgery*. 1984;5:107-117. <https://doi.org/10.1002/micr.1920050302>
38. Auer RN, Bell RB, Lee MA. Neuropathy with onion bulb formations and pure motor manifestations. *Can J Neurol Sci / J Can des Sci Neurol*. 1989;16:194-197. <https://doi.org/10.1017/S031716710028894>
39. Oh SJ, Claussen G, Odabasi Z, Palmer CP. Multifocal demyelinating motor neuropathy: pathologic evidence of 'inflammatory demyelinating polyradiculoneuropathy'. *Neurology*. 1995;45:1828-1832. <https://doi.org/10.1212/WNL.45.10.1828>
40. Sasaki M, Ohara S, Oide T, Hayashida K, Hayashi R. An autopsy case of chronic inflammatory demyelinating polyradiculoneuropathy with respiratory failure. *Muscle Nerve*. 2004;30:382-387. <https://doi.org/10.1002/mus.20072>
41. Koike H, Nishi R, Ikeda S, et al. Ultrastructural mechanisms of macrophage-induced demyelination in CIDP. *Neurology*. 2018;91:1051-1060. <https://doi.org/10.1212/WNL.0000000000006625>
42. Franssen H, Straver DCG. Pathophysiology of immune-mediated demyelinating neuropathies-part I: neuroscience. *Muscle Nerve*. 2013;48:851-864. <https://doi.org/10.1002/mus.24070>
43. Franssen H, Straver DCG. Pathophysiology of immune-mediated demyelinating neuropathies-Part II: neurology. *Muscle Nerve*. 2014;49:4-20. <https://doi.org/10.1002/mus.24068>
44. Garg N, Park SB, Howells J, et al. Conduction block in immune-mediated neuropathy: paranodopathy versus axonopathy. *Eur J Neurol*. 2019;26:1121-1129. <https://doi.org/10.1111/ene.13953>
45. Yan Aung W, Mar S, Benzinger TL. DTI as biomarker in axonal and myelin damage. *Imaging Med*. 2013;5(5):427-440. <https://doi.org/10.2217/iim.13.49>
46. Van Asseldonk JTH, Van Den Berg LH, Kalmijn S, et al. Axon loss is an important determinant of weakness in multifocal motor neuropathy. *J Neurol Neurosurg Psychiatry*. 2006;77(6):743-747. <https://doi.org/10.1136/jnnp.2005.064816>
47. Goedee H. *High-resolution ultrasound in diagnosis of polyneuropathies*. In: ISBN 9789462336841; 2017:167-190.
48. Kerasnoudis A, Pitarokouli K, Behrendt V, Gold R, Yoon MS. Correlation of nerve ultrasound, electrophysiological and clinical findings in chronic inflammatory demyelinating polyneuropathy. *J Neuroimaging*. 2015;25:207-216.
49. Kerasnoudis A, Voitalla D, Gold R, Pitarokouli K, Yoon MS. Multifocal motor neuropathy: correlation of nerve ultrasound, electrophysiological, and clinical finding. *J Peripher Nerv Syst*. 2014;347:129-136.
50. Rajabally YA, Morlese J, Kathuria D, Khan A. Median nerve ultrasonography in distinguishing neuropathy sub-types: a pilot study. *Acta Neurol Scand*. 2012;125:254-259.
51. Beekman R, Van Den Berg LH, Franssen H, Visser LH, Van Asseldonk JTH, Wokke JHJ. Ultrasonography shows extensive nerve enlargements in multifocal motor neuropathy. *Neurology*. 2005;65:305-307.
52. Vos SB, Jones DK, Viergever MA, Leemans A. Partial volume effect as a hidden covariate in DTI analyses. *NeuroImage*. 2011;55(4):1566-1576. <https://doi.org/10.1016/j.neuroimage.2011.01.048>
53. Oudeman J, Verhamme C, Engbersen MP, et al. Diffusion tensor MRI of the healthy brachial plexus. *PLoS One*. 2018;13:1-15. <https://doi.org/10.1371/journal.pone.0196975>

How to cite this article: van Rosmalen MH, Goedee HS, Derks R, et al. Quantitative magnetic resonance imaging of the brachial plexus shows specific changes in nerve architecture in chronic inflammatory demyelinating polyneuropathy, multifocal motor neuropathy and motor neuron disease. *Eur J Neurol*. 2021;28:2716-2726. <https://doi.org/10.1111/ene.14896>